Int. J. Anal. Appl. (2026), 24:165

International Journal of Analysis and Applications

Bifurcation analysis and Control in a Discrete-Time Predator-Prey Model with Smith-Type Growth and Monod-Haldane Response

A. A. Elsadany[1,*], Abdulaziz Almaslokh[1], B. Alreshidi[1], Ibrahim M. E. Abdelstar[2]

[1]*Department of Mathematics, College of Sciences and Humanities in Al-Kharj, Prince Sattam Bin Abdulaziz University, Al-Kharj, 11942, Saudi Arabia*

[2]*Department of Mathematics, Faculty of Science, Al-Azhar University, Nasr City, P.O.Box: 11884, Cairo, Egypt*

[*]*Corresponding author:* aelsadany1@yahoo.com

Abstract. This work examines a discrete-time predator-prey model that integrates Smith-type prey development and a Monod-Haldane functional response, which includes density-dependent regulation and non-monotonic predation effects. A thorough dynamical study is performed in three phases. First, the existence and local stability of all biologically viable equilibria extinction, predator-free, and coexistence states are demonstrated, uncovering regimes of extinction, stable coexistence, and oscillatory dynamics. Second, a thorough bifurcation analysis reveals important dynamic transitions, such as flip and Neimark-Sacker bifurcations. Two-parameter diagrams show how ecological factors affect system stability and persistence. We suggest an optimal control technique to control based on the chaos that is showing up in the bifurcation diagrams. For the best solutions, we use Pontryagin's maximal principle. This lets us use adaptive threshold control to keep the model stable. Finally, the numerical simulations confirmed the theoretical findings.

1. Introduction

Over the past two decades, mathematical modeling has become a vital tool for understanding how populations evolve and how ecosystems function. This shift has led to the development of a wide range of theoretical approaches in ecology. At the heart of many of these models is the Lotka-Volterra framework, which remains a foundational concept in studying predator-prey interactions [1, 2]. Building on this classic model, researchers have introduced increasingly sophisticated approaches to better capture the complexity of species interactions. These include various types of functional responses, such as Holling-type models [3], ratio-dependent (Michaelis-Menten) formulations [4], and Ivlev-type dynamics [5]. Over the years, these models have been extensively studied [6], with the goal

Received: Feb. 13, 2026.

2020 *Mathematics Subject Classification.* 39A10, 34K18, 37GK15, 39A11.

Key words and phrases. predator-prey dynamics; Smith growth function; bifurcation theory; optimal control; discrete-time systems; ecological management.

https://doi.org/10.28924/2291-8639-24-2026-165
ISSN: 2291-8639

of incorporating key ecological features like population structure, age distribution, and interactions between species. In ecosystems with multiple species, external influences such as seasonal cycles, time delays, and human activities like harvesting can lead to regular population cycles or even chaotic patterns [7]. Additionally, density-dependent factors often trigger bifurcations, which can increase the complexity and instability of ecological systems [8]. Interestingly, the presence of prey refuges areas where prey can hide from predators can help stabilize these systems by reducing predation pressure and making ecological dynamics more resilient [9].

Discrete-time modeling offers a suitable framework for ecological systems characterized by non-overlapping generations and seasonal breeding cycles [10]. Discrete models are well-known for having a wide range of difficult dynamics, such as period-doubling bifurcations, Neimark-Sacker bifurcations, and chaotic regimes. These dynamics are often less distinct in continuous-time models [11]. Discrete systems are important for the environment, but they also have a lot of analytical and computational advantages. For example, they make it possible to directly use bifurcation theory and chaos control techniques [12]. This strategy also works in real-life ecological management because conservation and harvesting measures are frequently done at certain times.In natural ecosystems, prey species frequently exhibit density-dependent defensive mechanisms, whereby an augmentation in population size enhances their collective ability to withstand predation or seek refuge, hence diminishing predation rates. We analyze these dynamics using a discrete-time, fractional-order predator-prey model that includes Smith growth and a Monod-Haldane functional response. The model is derived from the subsequent continuous-time system [13]:

$$\begin{aligned} \frac{dM(t)}{dt} &= \frac{M(1-M)}{1+\beta M} - \frac{\mu MH}{M^2+\sigma}, \\ \frac{dH(t)}{dt} &= \eta H\left(1 - \frac{H}{M^2+\sigma}\right), \end{aligned} \tag{1.1}$$

where M and H stand for the population densities of the predator and prey, respectively. The parameter η represents the predator's inherent growth rate (indicating predation intensity), whereas σ functions as a saturation constant. We use the forward Euler method with step size δ to discretize system (1.1) so that we can do numerical analysis and account for generations that don't overlap. This gives us the discrete-time system:

$$\begin{aligned} M_{n+1} &= M_n + \delta M_n\left(\frac{1-M_n}{1+\beta M_n} - \frac{\mu H_n}{M_n^2+\sigma}\right), \\ H_{n+1} &= H_n + \delta\eta H_n\left(1 - \frac{H_n}{M_n^2+\sigma}\right). \end{aligned} \tag{1.2}$$

The forward Euler scheme is chosen because it is easy to implement, works well with computers, and is easy to analyze, making it a strong base for studying system dynamics.

This study builds on the work of [14] by adding a discrete-time framework that comes from a fractional-order system. We find enough conditions for solutions to exist, look at equilibrium points and their long-term stability, and come up with criteria for reverse bifurcations and chaotic dynamics.

The main goal is to explain these complicated behaviors so that we may come up with ways to stop pathological oscillations.

The paper is organized as follows. Section 2 addresses non-negativity and boundedness. Section 3 presents the stability analysis of equilibria. Section 4 details the conditions for flip, Neimark-Sacker, and codimension-2 bifurcations. Optimal control analysis is studied in Section 5. Numerical simulations are provided in Section 6, followed by a discussion of the results in Section 7.

2. Non-Negativity and Boundedness

This section characterizes the system's non-negativity and boundedness of system (1.2).

Theorem 1. *For small step size δ the solution M_n, H_n of* (1.2) *are non-negative and bounded.*

Proof. Consider the discrete-time dynamical system (1.2) with initial conditions $M_0 \geq 0, H_0 \geq 0$, and parameters $\delta > 0, \beta \geq 0, \mu > 0, \sigma > 0, \eta > 0$.

We prove that for sufficiently small $\delta > 0$, the solutions remain non-negative and bounded for all $n \geq 0$. We rewrite the system as:

$$M_{n+1} = M_n \left[1 + \delta A_n\right],$$
$$H_{n+1} = H_n \left[1 + \delta B_n\right],$$

where

$$A_n = \frac{1 - M_n}{1 + \beta M_n} - \frac{\mu H_n}{M_n^2 + \sigma}, \quad B_n = \eta\left(1 - \frac{H_n}{M_n^2 + \sigma}\right).$$

We prove by induction that if $M_0 \geq 0$ and $H_0 \geq 0$, then $M_n \geq 0$ and $H_n \geq 0$ for all n.

First step: at $n = 0$, given $M_0 \geq 0, H_0 \geq 0$.

Second (Inductive) step: Assume $M_n \geq 0, H_n \geq 0$.

Third step: We show $M_{n+1} \geq 0, H_{n+1} \geq 0$.

From the reformulation:

$$M_{n+1} = M_n \left[1 + \delta A_n\right], \quad H_{n+1} = H_n \left[1 + \delta B_n\right].$$

If $(M_n, H_n) = (0, 0)$, then $M_{n+1} = 0 \geq 0$ and $H_{n+1} = 0 \geq 0$.

If $M_n > 0$ $(H_n > 0)$, then to ensure $M_{n+1} \geq 0$ $(H_{n+1} \geq 0)$, we need $1 + \delta A_n \geq 0$ $(1 + \delta B_n \geq 0)$.

We will find bounds on A_n and B_n after establishing boundedness. From the M-equation:

$$M_{n+1} = M_n + \delta\left[\frac{M_n(1 - M_n)}{1 + \beta M_n} - \frac{\mu M_n H_n}{M_n^2 + \sigma}\right]$$
$$\leq M_n + \delta \cdot \frac{M_n(1 - M_n)}{1 + \beta M_n}.$$

Let $f(M) = \frac{M(1-M)}{1+\beta M}$ for $M \geq 0$, then,:

$$f(M)\begin{cases} > 0 & \text{for } 0 < M < 1, \\ = 0 & \text{at } M = 0 \text{ and } M = 1, \\ < 0 & \text{for } M > 1. \end{cases}$$

If $M_n > 1$, then $f(M_n) < 0$, so $M_{n+1} < M_n$. If $M_n < 1$, $f(M_n) > 0$, so $M_{n+1} > M_n$, but it cannot grow beyond 1 because $f(M)$ becomes negative for $M > 1$.

For large M_n, $f(M_n) \approx -\frac{1}{\beta}M_n$ (since $1 + \beta M_n \approx \beta M_n$ and $1 - M_n \approx -M_n$), so:

$$M_{n+1} \approx M_n\left(1 - \frac{\delta}{\beta}\right),$$

which decreases geometrically if $\delta < \beta$. Thus, M_n is bounded above by some $U_M > 0$. In fact, we can take $U_M = \max(M_0, 1)$.

From the H-equation:

$$H_{n+1} = H_n + \delta\eta H_n\left(1 - \frac{H_n}{C_n}\right),$$

where $C_n = M_n^2 + \sigma \geq \sigma > 0$, and $C_n \leq U_M^2 + \sigma = L$.

Rewriting:

$$H_{n+1} = H_n\left[1 + \delta\eta - \frac{\delta\eta}{C_n}H_n\right].$$

This is a logistic-type map. The maximum possible value of H_{n+1} for fixed C_n occurs at:

$$H_n = \frac{C_n(1+\delta\eta)}{2\delta\eta},$$

yielding:

$$H_{n+1} \leq \frac{C_n(1+\delta\eta)^2}{4\delta\eta} \leq \frac{L(1+\delta\eta)^2}{4\delta\eta} = K_H.$$

Thus, $H_n \leq K_H$ for all n. We now have uniform bounds:

$$0 \leq M_n \leq U_M, \quad 0 \leq H_n \leq K_H.$$

We compute bounds for A_n and B_n:

- $A_n \geq \frac{1-U_M}{1+\beta U_M} - \frac{\mu K_H}{\sigma} = m_A$,
- $B_n \geq \eta\left(1 - \frac{K_H}{\sigma}\right) = m_B$.

Then:

$$M_{n+1} = M_n(1 + \delta A_n) \geq M_n(1 + \delta m_A),$$
$$H_{n+1} = H_n(1 + \delta B_n) \geq H_n(1 + \delta m_B).$$

Choose δ small enough so that:

$$1 + \delta m_A > 0, \quad 1 + \delta m_B > 0.$$

Then: If

$$M_n \begin{cases} > 0, & \text{then } M_{n+1} > 0, \\ = 0, & \text{then } M_{n+1} = 0 \end{cases}$$

and

$$H_n \begin{cases} > 0, & \text{then } H_{n+1} > 0, \\ = 0, & \text{then } H_{n+1} = 0 \end{cases}$$

Thus, non-negativity is preserved. Moreover, if $M_0 > 0$ and $H_0 > 0$, then positivity is preserved for all n.

For sufficiently small $\delta > 0$, the system satisfies:

- Non-negativity: $M_n \geq 0$, $H_n \geq 0$ for all n
- If $M_0 > 0$ and $H_0 > 0$, then positivity: $M_n > 0$, $H_n > 0$ for all n
- Boundedness: $M_n \leq U_M$, $H_n \leq K_H$ for all n

□

3. Dynamical Behaviors of the Discrete-Time Predator-Prey Model

3.1. **Stability analysis.** This section investigates the local stability analysis of steady state points of the model (1.2). Obviously, the model (1.2) equilibrium solutions correspond to the following population states:

(1) $P_0 = (0, 0)$ signifies the state of complete extinction for both species,
(2) $P_1 = (1, 0)$ denotes a scenario where the predator population is eradicated,
(3) $P_2 = (0, \sigma)$ indicates the collapse of the prey population,
(4) $P_3 = (M_3, H_3) = (\dfrac{1-\mu}{1+\beta\mu}, M_3^2 + \sigma)$ represents a non-trivial equilibrium where prey and predator populations coexist.

We note that P_0, P_1 and P_2 are always exist, but P_3 exist if $\mu < 1$.
To analyze the behavior dynamic of system (1.2), we calculate the linearization matrix $J(P)$ of (1.2) at any point $P^* = (M^*, H^*)$

$$J(P) = \begin{pmatrix} 1 + \delta\left(\frac{1-M^2\beta-2M}{(M\beta+1)^2} + \frac{\mu H(M^2-\sigma)}{(M^2+\sigma)^2}\right) & \frac{-\delta\mu M}{M^2+\sigma} \\ \frac{2\delta\eta H^2 M}{(M^2+\sigma)^2} & 1 + \delta\eta\left(1 - \frac{2H}{M^2+\sigma}\right) \end{pmatrix}. \tag{3.1}$$

Theorem 2. *P_0 is always unstable.*

Proof. Substituting by $P_0 = (0, 0)$ into (3.1), the Jacobian matrix at P_0 can be written as

$$J(P_0) = \begin{pmatrix} 1+\delta & 0 \\ 0 & 1+\delta\eta \end{pmatrix}. \tag{3.2}$$

$J(P_0)$ has two eigenvalues are $\xi_{01} = 1 + \delta$ and $\xi_{02} = 1 + \delta\eta$. Since all parameters are positive, then ξ_{01} and ξ_{02} are always positive. Therefore P_0 is always unstable. □

For the second equilibrium point P_1, we introduce the following theorem.

Theorem 3. *P_1 is always unstable.*

Proof. Substituting by $P_1 = (1, 0)$ into (3.1), the Jacobian matrix at P_0 can be written as

$$J(P_1) = \begin{pmatrix} 1 - \frac{\delta}{\beta+1} & -\frac{\delta\mu}{\sigma+1} \\ 0 & 1 + \delta\eta \end{pmatrix}. \tag{3.3}$$

$J(P_1)$ has two eigenvalues are $\xi_{11} = 1 - \frac{\delta}{\beta+1}$ and $\xi_{12} = 1 + \delta\eta > 0$. Therefore P_1 is always unstable. □

For the third equilibrium point P_2, we introduce the following theorem.

Theorem 4. *The stability of the fixed point P_2 is determined as follows:*

(i): *Asymptotically stable (sink) if* $0 < \delta < \min\left\{\frac{2}{1-\mu}, \frac{2}{\eta}\right\}$,

(ii): *Unstable (source) if* $\delta > \max\left\{\frac{2}{1-\mu}, \frac{2}{\eta}\right\}$,

(iii): *Unstable (saddle) if* $\min\left\{\frac{2}{1-\mu}, \frac{2}{\eta}\right\} < \delta < \max\left\{\frac{2}{1-\mu}, \frac{2}{\eta}\right\}$,

(iv): *Non-hyperbolic if* $\delta \in \left\{\frac{2}{1-\mu}, \frac{2}{\eta}\right\}$.

Proof. Substituting by $P_2 = (0, \sigma)$ into (3.1), the Jacobian matrix at P_0 can be written as

$$J(P_2) = \begin{pmatrix} 1 - \delta(1-\mu) & 0 \\ 0 & 1 - \delta\eta \end{pmatrix}. \tag{3.4}$$

$J(P_2)$ has two eigenvalues are $\xi_{21} = 1 - \delta(1-\mu)$ and $\xi_{22} = 1 - \delta\eta$. Therefore, by some calculation we can get the results (i)-(iv). □

To study the stability of interior point E_1 of the system (1.2), we recall the following Lemma.

Lemma 1. *[15] let $F(\xi) = \xi^2 - Tr\xi + Det$ is the characteristic equation of jacobian matrix $J(P^*)$. Suppose that $F(1) > 0, \xi_1, \xi_2$ are the two roots of $F(\xi) = 0$. Then,*

(i): *$|\xi_1| < 1$ and $|\xi_2| < 1$ (P^* is asymptotically stable) if and only if $F(-1) > 0$ and $Det < 1$;*

(ii): *$|\xi_1| > 1$ and $|\xi_2| > 1$ (P^* is source) if and only if $F(-1) > 0$ and $Det > 1$;*

(iii): *$|\xi_1| < 1$ and $|\xi_2| > 1$ or $(|\xi_1| > 1$ and $|\xi_2| < 1)$ (P^* is saddle) if and only if $F(-1) < 0$;*

(iv): *$\xi_1 = -1$ and $\xi_2 \neq 1$ if and only if $F(-1) = 0$ and $Tr \neq 0, 2$;*

(v): *ξ_1 and ξ_2 are complex and $|\xi_{1,2}| = 1$ if and only if $Tr^2 - 4Det < 0$ and $Det = 1$.*

By Lemma (1), the following can be accomplished.

Theorem 5. *P_3 is*

(i): *Asymptotically stable (sink) if one of the following conditions holds:*

(i.1): *$\Delta \geqslant 0$ and $0 < \delta < \delta_1$.*

(i.2): *$\Delta < 0$ and $0 < \delta < \delta_2$.*

(ii): *Unstable (source) if one of the following conditions holds:*

(ii.1): *$\Delta \geqslant 0$ and $\delta > \delta_3$.*

(ii.2): $\Delta < 0$ *and* $\delta > \delta_2$.

(iii): *Unstable (saddle) if* $\Delta \geqslant 0$ *and* $\delta_1 < \delta < \delta_3$.

(iv): *Non-hyperbolic if one of the following conditions holds:*

(iv.1): $\Delta \geqslant 0$ *and* $\delta = \delta_1$ *or* δ_3.

(iv.2): $\Delta < 0$ *and* $\delta = \delta_2$.

where $\delta_1 = \dfrac{B - \sqrt{\Delta}}{A}$, $\delta_2 = \dfrac{B}{A}$ $\delta_3 = \dfrac{B + \sqrt{\Delta}}{A}$ *and* $\Delta = B^2 - 4A$.

Proof. The Jacobian matrix of P_3 can be written as

$$J(P_3) = \begin{pmatrix} 1 - \delta\left(\frac{M_3^4\beta + 2M_3^2 - 1}{(M_3^2\beta+1)^2} + \frac{\mu(M_3+\sigma)(\sigma - M_3^4)}{(M_3^4+\sigma)^2}\right) & \frac{-\delta\mu M_3^2}{M_3^4+\sigma} \\ \frac{2\delta\eta(M_3+\sigma)^2 M_3^2}{(M_3^4+\sigma)^2} & 1 - \frac{\delta\eta\left(\sigma + 2M_3 - M_3^4\right)}{M_3^4+\sigma} \end{pmatrix}.$$

The characteristic equation of $J(P_3)$ has the form

$$F(\xi) = \xi^2 - Tr_3\xi + Det_3, \tag{3.5}$$

where

$$\begin{aligned} Tr_3 &= 2 - B\delta, \\ Det_3 &= A\delta^2 - B\delta + 1, \\ A &= Det\begin{pmatrix} \frac{M_3^4\beta + 2M_3^2 - 1}{(M_3^2\beta+1)^2} + \frac{\mu(M_3+\sigma)(\sigma - M_3^4)}{(M_3^4+\sigma)^2} & \frac{-\mu M_3^2}{M_3^4+\sigma} \\ \frac{2\eta(M_3+\sigma)^2 M_3^2}{(M_3^4+\sigma)^2} & \frac{\eta\left(\sigma + 2M_3 - M_3^4\right)}{M_3^4+\sigma} \end{pmatrix}. \\ B &= \frac{M_3^4\beta + 2M_3^2 - 1}{(M_3^2\beta+1)^2} + \frac{\mu(M_3+\sigma)(\sigma - M_3^4)}{(M_3^4+\sigma)^2} + \frac{\eta\left(\sigma + 2M_3 - M_3^4\right)}{M_3^4+\sigma} \end{aligned}$$

Then, from (3.5) we have $F(-1) = A\delta^2 - 2B\delta + 4$ and $Det_3 = A\delta^2 - B\delta + 1$. Applying the Lemma (1), stability conditions (i)-(iv) are achieved. □

Define

$$\begin{aligned} \Phi_1 &= \{(\delta, \beta, \mu, \sigma, \eta) : \delta = \delta_1, \Delta \geq 0\}, \\ \Phi_2 &= \{(\delta, \beta, \mu, \sigma, \eta) : \delta = \delta_2, \Delta < 0\}, \\ \Phi_3 &= \{(\delta, \beta, \mu, \sigma, \eta) : \delta = \delta_3, \Delta \geq 0\}. \end{aligned}$$

Based on the preceding analysis, the bifurcation behavior at the equilibrium point P_3 is characterized as follows:

If condition (iv.1) of Theorem (5) is satisfied, then the Jacobian matrix $J(P_3)$ has one eigenvalue equal to -1 while the other eigenvalue is distinct from both 1 and -1. This condition corresponds to the parameter configuration:

$$(\delta, \beta, \mu, \sigma, \eta) \in \Phi_1 \cup \Phi_3.$$

When the parameter δ varies in a neighborhood of either δ_1 (with $(\delta, \beta, \mu, \sigma, \eta) \in \Phi_1$) or δ_3 (with $(\delta, \beta, \mu, \sigma, \eta) \in \Phi_3$), system (1.2) undergoes a flip bifurcation at P_3.

If condition (iv.2) holds, then $J(P_3)$ possesses a pair of complex conjugate eigenvalues with modulus 1, indicating that:

$$(\delta, \beta, \mu, \sigma, \eta) \in \Phi_2.$$

When δ varies near the critical value δ_2 while maintaining $(\delta, \beta, \mu, \sigma, \eta) \in \Phi_2$, system (1.2) exhibits a Neimark-Sacker bifurcation at P_3.

4. Bifurcation Analysis

This section presents the analysis of flip (period-doubling) and Neimark-Sacker bifurcations at the equilibrium point P_3. The center manifold theorem is applied to reduce the system dynamics and study the flip bifurcation, while the normal form method is used to characterize the Neimark-Sacker bifurcation.

4.1. **Flip Bifurcation.** We analyze the flip bifurcation at P_3 when the parameters $(\delta, \beta, \mu, \sigma, \eta)$ vary within a small neighborhood of the critical set Φ_1 (or Φ_3). Let δ_* denote a small perturbation parameter such that the bifurcation parameter δ is varied as $\delta \to \delta + \delta_*$. The perturbed system corresponding to (1.2) is:

$$\begin{aligned} M_{n+1} &= M_n + (\delta + \delta_*) M_n \left(\frac{1 - M_n}{1 + \beta M_n} - \frac{\mu H_n}{M_n^2 + \sigma} \right), \\ H_{n+1} &= H_n + (\delta + \delta_*) \eta H_n \left(1 - \frac{H_n}{M_n^2 + \sigma} \right). \end{aligned} \tag{4.1}$$

Translating $P_3(M_3, H_3)$ to the origin via $U_n = M_n - M_3$ and $V_n = H_n - H_3$, system (4.1) becomes

$$\begin{pmatrix} U_{n+1} \\ V_{n+1} \end{pmatrix} = \begin{pmatrix} a_{11} U_n + a_{12} V_n + a_{13} U_n V_n + (b_{11} U_n + b_{12} V_n + b_{13} U_n V_n)\, \delta_* + O((|U_n| + |V_n|)^3) \\ a_{21} U_n + a_{22} V_n + a_{23} U_n V_n + (b_{21} U_n + b_{22} V_n + b_{23} U_n V_n)\, \delta_* + O((|U_n| + |V_n|)^3) \end{pmatrix}, \tag{4.2}$$

where the coefficients are

$$\begin{aligned} a_{11} &= 1 + \delta \left(-4M_3^3\beta^2 + 3M_3^2\beta^2 + 3M_3^2\beta - 2M_3\beta - 2M_3 + 1 + \frac{2\mu M_3^2 H_3}{\sigma^2} - \mu H_3 \left(\frac{1}{\sigma} - \frac{M_3^2}{\sigma^2} \right) \right), \\ a_{12} &= -\delta \mu M_3 \left(\frac{1}{\sigma} - \frac{M_3^2}{\sigma^2} \right), \quad a_{13} = \delta \left(\frac{2\mu M_3^2}{\sigma^2} - \mu \left(\frac{1}{\sigma} - \frac{M_3^2}{\sigma^2} \right) \right), \\ b_{11} &= M_3(1 - M_3)(2M_3\beta^2 - \beta) + (-2M_3 + 1)(M_3^2\beta^2 - M_3\beta + 1) + \frac{2\mu M_3^2 H_3}{\sigma^2} - \mu H_3 \left(\frac{1}{\sigma} - \frac{M_3^2}{\sigma^2} \right), \\ b_{12} &= -\mu M_3 \left(\frac{1}{\sigma} - \frac{M_3^2}{\sigma^2} \right), \quad b_{13} = \frac{2\mu M_3^2}{\sigma^2} - \mu \left(\frac{1}{\sigma} - \frac{M_3^2}{\sigma^2} \right), \quad a_{21} = \frac{2\delta \eta H_3^2 M_3}{\sigma^2}, \\ a_{22} &= 1 + \delta \eta H_3 \left(-\frac{1}{\sigma} + \frac{M_3^2}{\sigma^2} \right) + \delta \eta \left(1 - H_3 \left(\frac{1}{\sigma} - \frac{M_3^2}{\sigma^2} \right) \right), \quad a_{23} = \frac{4\delta \eta H_3 M_3}{\sigma^2}, \quad b_{21} = \frac{2\eta H_3^2 M_3}{\sigma^2}, \\ b_{22} &= \eta \left(1 - H_3 \left(\frac{1}{\sigma} - \frac{M_3^2}{\sigma^2} \right) \right), \quad b_{23} = \frac{4\eta H_3 M_3}{\sigma^2}. \end{aligned}$$

Let $S_1 = \begin{pmatrix} a_{11} & a_{12} \\ a_{21} & a_{22} \end{pmatrix}$. Its eigenvalues are ρ_1 and ρ_2, with $\rho_1 = -1$ and $|\rho_2| \neq 1$ at the bifurcation. Corresponding eigenvectors are

$$\mathbf{v}_1 = \begin{pmatrix} a_{12} \\ -1 - a_{11} \end{pmatrix}, \quad \mathbf{v}_2 = \begin{pmatrix} a_{12} \\ \rho_2 - a_{11} \end{pmatrix}.$$

Define the invertible matrix $S_2 = (\mathbf{v}_1 \ \mathbf{v}_2) = \begin{pmatrix} a_{12} & a_{12} \\ -1 - a_{11} & \rho_2 - a_{11} \end{pmatrix}$. Applying the transformation $\begin{pmatrix} U_n \\ V_n \end{pmatrix} = S_2 \begin{pmatrix} x_n \\ y_n \end{pmatrix}$ to (4.2) yields

$$\begin{pmatrix} x_{n+1} \\ y_{n+1} \end{pmatrix} = \begin{pmatrix} -1 & 0 \\ 0 & \rho_2 \end{pmatrix} \begin{pmatrix} x_n \\ y_n \end{pmatrix} + S_2^{-1} \begin{pmatrix} f_1(U_n, V_n, \delta_*) \\ f_2(U_n, V_n, \delta_*) \end{pmatrix},$$

where

$$\begin{aligned} f_1(U_n, V_n, \delta_*) &= a_{13} U_n V_n + (b_{11} U_n + b_{12} V_n + b_{13} U_n V_n)\delta_*, \\ f_2(U_n, V_n, \delta_*) &= a_{23} U_n V_n + (b_{21} U_n + b_{22} V_n + b_{23} U_n V_n)\delta_*, \\ U_n &= a_{12}(x_n + y_n), \\ V_n &= -(1 + a_{11})x_n + (\rho_2 - a_{11}) y_n. \end{aligned}$$

Thus, we obtain the system

$$\begin{pmatrix} x_{n+1} \\ y_{n+1} \end{pmatrix} = \begin{pmatrix} -1 & 0 \\ 0 & \rho_2 \end{pmatrix} \begin{pmatrix} x_n \\ y_n \end{pmatrix} + \begin{pmatrix} Q_1(x_n, y_n, \delta_*) \\ Q_2(x_n, y_n, \delta_*) \end{pmatrix}, \tag{4.3}$$

with

$$Q_1(x_n, y_n, \delta_*) = \frac{1}{\rho_2 + 1}\left[\frac{\rho_2 - a_{11}}{a_{12}} f_1 - f_2\right], \quad Q_2(x_n, y_n, \delta_*) = \frac{1}{\rho_2 + 1}\left[\frac{1 + a_{11}}{a_{12}} f_1 + f_2\right].$$

The center manifold $W^c(0,0,0)$ of (4.3) at $(0,0)$ in a small neighborhood of $\delta_* = 0$ can be expressed as

$$W^c(0,0,0) = \left\{(x_n, y_n, \delta_*) \in \mathbb{R}^3 : x_n = g(y_n, \delta_*),\ g(0,0) = 0,\ Dg(0,0) = 0\right\},$$

where, for sufficiently small y_n and δ_*,

$$x_n = g(y_n, \delta_*) = e_2 y_n^2 + e_1 \delta_* y_n + O\left((|y_n| + |\delta_*|)^3\right).$$

The function g must satisfy the invariance equation

$$g\left(-y_n + Q_2(y_n, g(y_n, \delta_*)), \delta_*\right) = \rho_2\, g(y_n, \delta_*) + Q_1(y_n, g(y_n, \delta_*), \delta_*). \tag{4.4}$$

Equating coefficients of like powers in (4.4) gives

$$e_2 = \frac{(\rho_2 - a_{11})(a_{11}a_{13} + a_{12}a_{23} - a_{13}\rho_2)}{\rho_2^2 - 1}, \quad e_1 = \frac{(a_{11}b_{13} + a_{12}b_{23} + b_{13})(\rho_2 - 2a_{11} - 1)}{(1 + a_{11})(a_{11}a_{13} + a_{12}a_{23} + a_{13})}.$$

On the center manifold, the dynamics are governed by the one-dimensional map

$$f(y_n) = -y_n + \varphi_1 y_n \delta_* + \varphi_2 y_n \delta_*^2 + \varphi_3 y_n^2 + \varphi_4 y_n^2 \delta_* + \varphi_5 y_n^3 + O\left((|y_n| + |\delta_*|)^4\right), \tag{4.5}$$

where the coefficients φ_i are

$$\varphi_1 = \frac{1}{a_{12}(\rho_2+1)}\Big\{b_{21}a_{12}^2 - b_{12}(\rho_2-a_{11})^2 \quad + a_{12}\Big[-e_1\rho_2^2 + (-2e_1 - b_{11} + b_{22})\rho_2 + (b_{11}-b_{22})a_{11} - e_1\Big]\Big\},$$

$$\varphi_2 = \frac{e_1}{a_{12}(\rho_2+1)}\Big\{2a_{12}^2 b_{21} - \Big[(b_{11}-b_{22})(\rho_2 - 2a_{11} - 1)a_{12}\Big] + 2b_{12}(1+a_{11})(\rho_2 - a_{11})\Big\},$$

$$\varphi_3 = \frac{1}{\rho_2+1}\Big[(-e_2 - a_{13})\rho_2^2 + (2a_{11}a_{13} + a_{12}a_{23})\rho_2 - a_{13}a_{11}^2 - a_{11}a_{12}a_{23} + e_2\Big],$$

$$\begin{aligned}\varphi_4 = \frac{1}{a_{12}(\rho_2+1)}\Big\{ &- e_2 b_{12}(1+a_{11})(\rho_2 - a_{11}) + a_{12}^2\Big[a_{11}(-3e_1a_{23} - b_{23}) + (2e_1a_{23} + b_{23})\rho_2 - e_1a_{23} - e_2b_{21}\Big] \\ &+ a_{12}\Big[a_{11}^2(-3e_1a_{13} - b_{13}) + a_{11}\Big((4e_1a_{13} + 2b_{13})\rho_2 + e_2(-b_{11} + b_{22}) - 2e_1a_{13}\Big) \\ &+ (-e_1a_{13} - b_{13})\rho_2^2 + \Big((-2b_{22} - b_{11})e_2 + 2e_1a_{13}\Big)\rho_2 - e_2(b_{22} + 2b_{11})\Big]\Big\},\end{aligned}$$

$$\varphi_5 = -e_2\Big[a_{13}(\rho_2 - a_{11}) + a_{23}a_{12}\Big].$$

The key discriminatory quantities for the flip bifurcation are defined as

$$\chi_1 = \left(\frac{\partial^2 f}{\partial y_n \partial \delta_*} + \frac{1}{2}\frac{\partial f}{\partial \delta_*}\frac{\partial^2 f}{\partial y_n^2}\right)\Big|_{(0,0)}, \quad \chi_2 = \left(\frac{1}{6}\frac{\partial^3 f}{\partial y_n^3} + \left(\frac{1}{2}\frac{\partial^2 f}{\partial y_n^2}\right)^2\right)\Big|_{(0,0)}. \tag{4.6}$$

From (4.5), we compute $\chi_1 = \varphi_1$ and $\chi_2 = \varphi_5 + \varphi_3^2$.

Based on the flip bifurcation theorem [16], we state the following result.

Theorem 6. *If $\chi_2 \neq 0$, then system* (4.1) *undergoes a flip bifurcation at P_3 as the parameter δ varies through the critical value in a small neighborhood of $(0,0)$. Moreover, the period-2 orbits bifurcating from P_3 are stable if $\chi_2 > 0$ and unstable if $\chi_2 < 0$.*

From Fig. (1)(a) it can be seen that P_3 is stable when $\delta < \delta_* = 0.3$ and loses its stability through flip bifurcation when $\delta > \delta_*$. We see that, when the parameter δ moving increasingly into $(0, 0.7)$, it should be noted that the parameters fixed here satisfy theorem (6).

To prove flip bifurcation exists, we drew Fig. (1)(b) and note that each (1)(a) and (1)(b) supports each other.

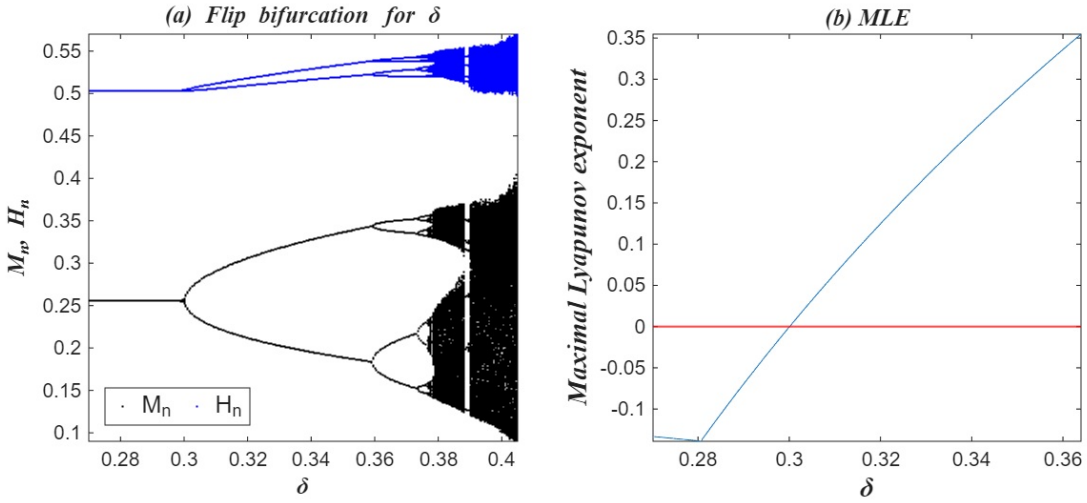

FIGURE 1. Flip bifurcation diagram and its corresponding Maximal Lyapunov exponent.

Phase portrait figure (2) below has the same parameter values of figure (1) to illustrate the effect of flip bifurcation on the phase portrait and shows how the prey population M_n evolves over time for different δ values. The parameter δ represents the time step size in the discrete-time model. Larger δ values generally lead to faster dynamics and potentially different equilibrium states. The Allee effect in the prey growth term causes complex nonlinear behavior.

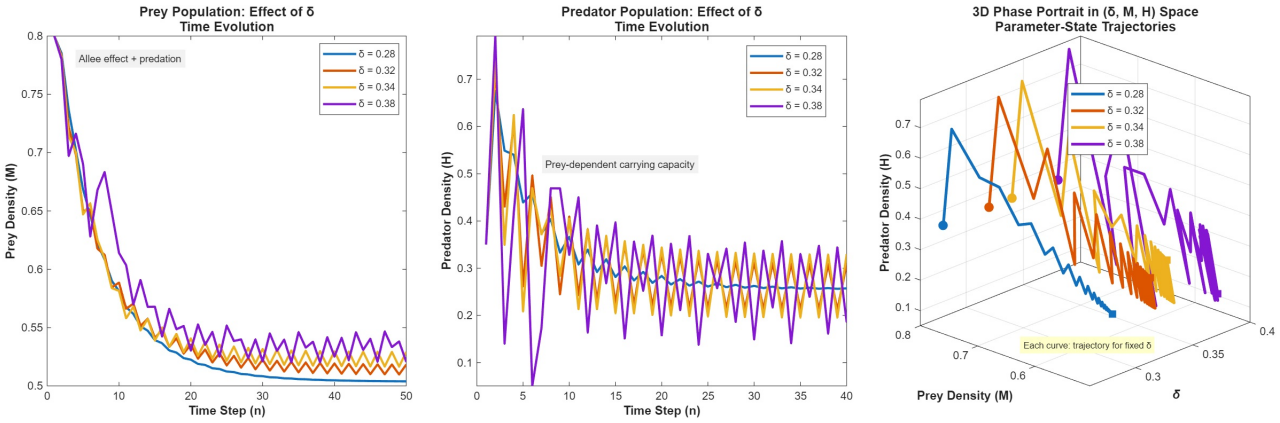

FIGURE 2. Effect of time step parameter δ.

Figures (2)(a) and (2)(b) shows predator population H_n dynamics. The predator growth depends on prey availability through the term $M_n^2 + \sigma$ in the denominator. Different δ values affect how quickly predators respond to changes in prey density. The coupling between predator and prey dynamics creates the oscillatory patterns observed in the plots.

Figure (2)(c) visualizes the trajectories in the combined parameter-state space. Each colored curve represents the system evolution for a specific δ value. The plot shows how trajectories evolve in the three-dimensional space, revealing the coupling between the time step parameter δ and the state variables M_n and H_n. The projection of trajectories onto different planes helps visualize relationships between variables.

4.2. **Neimark-Sacker Bifurcation.** A Neimark-Sacker (N-S) bifurcation at P_3 occurs when the parameters $(\delta, \beta, \mu, \sigma, \eta)$ lie in a small neighborhood of the critical set Φ_2. We introduce a small perturbation δ_* (with $|\delta_*| \ll 1$) such that $\delta \to \delta + \delta_*$. The perturbed system is

$$\begin{aligned} M_{n+1} &= M_n + (\delta + \delta_*) M_n \left(\frac{1 - M_n}{1 + \beta M_n} - \frac{\mu H_n}{M_n^2 + \sigma} \right), \\ H_{n+1} &= H_n + (\delta + \delta_*) \eta H_n \left(1 - \frac{H_n}{M_n^2 + \sigma} \right). \end{aligned} \tag{4.7}$$

Shifting $P_3(M_3, H_3)$ to the origin via $U_n = M_n - M_3$ and $V_n = H_n - H_3$ yields

$$\begin{pmatrix} U_{n+1} \\ V_{n+1} \end{pmatrix} = \begin{pmatrix} c_{11} U_n + c_{12} V_n + c_{13} U_n V_n + c_{14} U_n^2 + c_{15} V_n^2 + O((|U_n| + |V_n|)^3) \\ c_{21} U_n + c_{22} V_n + c_{23} U_n V_n + c_{24} U_n^2 + c_{25} V_n^2 + O((|U_n| + |V_n|)^3) \end{pmatrix}, \tag{4.8}$$

with coefficients

$$c_{11} = 1 + (\delta + \delta_*) \left(-4M_3^3\beta^2 + 3M_3^2\beta^2 + 3M_3^2\beta - 2M_3\beta - 2M_3 + 1 + \frac{\mu H_3 (3M_3^2 - \sigma)}{\sigma^2} \right),$$

$$c_{12} = -(\delta+\delta_*)\mu M_3\left(\frac{1}{\sigma}-\frac{M_3^2}{\sigma^2}\right),\ c_{13} = (\delta+\delta_*)\frac{\mu(3M_3^2-\sigma)}{\sigma^2},$$
$$c_{14} = (\delta+\delta_*)\left(-1+(-6M_3^2+3M_3)\beta^2+(3M_3-1)\beta+\frac{3\mu M_3 H_3}{\sigma^2}\right),$$
$$c_{15} = 0,\ c_{21} = 2(\delta+\delta_*)\frac{\eta H_3^2 M_3}{\sigma^2},\ c_{22} = 1+(\delta+\delta_*)\eta+\frac{-2H_3\eta(\delta+\delta_*)\sigma+2H_3M_3^2\eta(\delta+\delta_*)}{\sigma^2},$$
$$c_{23} = 4(\delta+\delta_*)\frac{\eta H_3 M_3}{\sigma^2},\ c_{24} = (\delta+\delta_*)\frac{\eta H_3^2}{\sigma^2},\ c_{25} = (\delta+\delta_*)\eta\left(\frac{M_3^2}{\sigma^2}-\frac{1}{\sigma}\right).$$

The characteristic equation of the linear part of (4.8) at $(0,0)$ is

$$\omega^2 + p(\delta_*)\omega + q(\delta_*) = 0, \tag{4.9}$$

where

$$p(\delta_*) = -2 - G(\delta+\delta_*),\quad q(\delta_*) = 1 + G(\delta+\delta_*) + S(\delta+\delta_*)^2,$$

with $G = c_{22}-c_{11}$ and $S = c_{21}c_{12}-c_{11}c_{22}$. For $(\delta,\beta,\mu,\sigma,\eta)\in\Phi_2$ and δ_* near 0, the roots of (4.9) are complex conjugates:

$$\omega_{1,2} = 1+\frac{G(\delta+\delta_*)}{2} \pm \frac{i(\delta+\delta_*)}{2}\sqrt{4S-G^2}.$$

Their modulus is $|\omega_{1,2}| = \sqrt{q(\delta_*)}$, and

$$\left.\frac{d|\omega_{1,2}|}{d\delta_*}\right|_{\delta_*=0} = -\frac{G}{2} > 0.$$

At the bifurcation ($\delta_* = 0$), we require $\omega_{1,2}^n \neq 1$ for $n = 1,2,3,4$, which is equivalent to $p(0)\neq -2,0,1,2$. Since $p^2(0)-4q(0) < 0$ and $q(0) = 1$, we have $p^2(0) < 4$, so $p(0)\neq \pm 2$ automatically. The conditions $p(0)\neq 0,1$ lead to

$$G^2 \neq 2S,\quad G^2 \neq 3S. \tag{4.10}$$

Thus, under (4.10), the eigenvalues at $(0,0)$ do not lie on the unit circle or on the real axes when $\delta_* = 0$.

To derive the normal form, let $\zeta = \mathrm{Re}(\omega_{1,2})$ and $\xi = \mathrm{Im}(\omega_{1,2})$ at $\delta_* = 0$. Define the transformation matrix

$$T = \begin{pmatrix} c_{12} & 0 \\ \zeta - c_{11} & -\xi \end{pmatrix} = \begin{pmatrix} c_{12} & 0 \\ -\frac{1}{2}G & -\frac{1}{2}(\delta\sqrt{4S-G^2}) \end{pmatrix}. \tag{4.11}$$

Applying $\begin{pmatrix} U_n \\ V_n \end{pmatrix} = T\begin{pmatrix} x_n \\ y_n \end{pmatrix}$ to (4.8) gives

$$\begin{pmatrix} x_{n+1} \\ y_{n+1} \end{pmatrix} = \begin{pmatrix} \zeta & -\xi \\ \xi & \zeta \end{pmatrix}\begin{pmatrix} x_n \\ y_n \end{pmatrix} + \begin{pmatrix} \tilde{f}(x_n,y_n) \\ \tilde{g}(x_n,y_n) \end{pmatrix}, \tag{4.12}$$

where

$$\tilde{f}(x_n,y_n) = c_{13}\left[(\zeta-c_{11})x_n^2 - \xi x_n y_n\right],$$
$$\tilde{g}(x_n,y_n) = [c_{13}(c_{11}-\zeta)+c_{12}c_{23}]\left[\frac{c_{11}-\zeta}{\xi}x_n^2 + x_n y_n\right],$$
$$U_n = c_{12}x_n,$$
$$V_n = (\zeta-c_{11})x_n - \xi y_n.$$

The second- and third-order partial derivatives at $(0,0)$ are

$$\begin{aligned}
&\frac{\partial^2 \tilde{f}}{\partial x_n^2} = 2c_{13}(\zeta - c_{11}), && \frac{\partial^2 \tilde{f}}{\partial x_n \partial y_n} = -\xi c_{13}, && \frac{\partial^2 \tilde{f}}{\partial y_n^2} = 0,\\
&\frac{\partial^2 \tilde{g}}{\partial x_n^2} = \frac{2(c_{11}-\zeta)}{\xi}\left[c_{13}(c_{11}-\zeta) + c_{12}c_{23}\right], && \frac{\partial^2 \tilde{g}}{\partial x_n \partial y_n} = c_{13}(c_{11}-\zeta) + c_{12}c_{23}, && \frac{\partial^2 \tilde{g}}{\partial y_n^2} = 0,
\end{aligned} \tag{4.13}$$

and all third derivatives are zero.

The critical discriminatory quantity $\hbar$ for the N-S bifurcation is

$$\hbar = -\operatorname{Re}\left[\frac{(1-2\omega)\overline{\omega}^2}{1-\omega}\zeta_{11}\zeta_{20}\right] - \frac{1}{2}|\zeta_{11}|^2 - |\zeta_{02}|^2 + \operatorname{Re}(\overline{\omega}\zeta_{21}), \tag{4.14}$$

where $\omega = \zeta + i\xi$ and

$$\begin{aligned}
\zeta_{11} &= \frac{1}{4}\left[\frac{\partial^2 \tilde{f}}{\partial x_n^2} + \frac{\partial^2 \tilde{f}}{\partial y_n^2} + i\left(\frac{\partial^2 \tilde{g}}{\partial x_n^2} - \frac{\partial^2 \tilde{g}}{\partial y_n^2}\right)\right]_{(0,0)},\\
\zeta_{20} &= \frac{1}{8}\left[\frac{\partial^2 \tilde{f}}{\partial x_n^2} - \frac{\partial^2 \tilde{f}}{\partial y_n^2} + 2\frac{\partial^2 \tilde{g}}{\partial x_n \partial y_n} + i\left(\frac{\partial^2 \tilde{g}}{\partial x_n^2} - \frac{\partial^2 \tilde{g}}{\partial y_n^2} - 2\frac{\partial^2 \tilde{f}}{\partial x_n \partial y_n}\right)\right]_{(0,0)},\\
\zeta_{02} &= \frac{1}{8}\left[\frac{\partial^2 \tilde{f}}{\partial x_n^2} - \frac{\partial^2 \tilde{f}}{\partial y_n^2} - 2\frac{\partial^2 \tilde{g}}{\partial x_n \partial y_n} + i\left(\frac{\partial^2 \tilde{g}}{\partial x_n^2} - \frac{\partial^2 \tilde{g}}{\partial y_n^2} + 2\frac{\partial^2 \tilde{f}}{\partial x_n \partial y_n}\right)\right]_{(0,0)},\\
\zeta_{21} &= \frac{1}{16}\left[\frac{\partial^3 \tilde{f}}{\partial x_n^3} + \frac{\partial^3 \tilde{f}}{\partial x_n \partial y_n^2} + \frac{\partial^3 \tilde{g}}{\partial x_n^2 \partial y_n} + \frac{\partial^3 \tilde{g}}{\partial y_n^3} + i\left(\frac{\partial^3 \tilde{g}}{\partial x_n^3} + \frac{\partial^3 \tilde{g}}{\partial x_n \partial y_n^2} - \frac{\partial^3 \tilde{f}}{\partial x_n^2 \partial y_n} - \frac{\partial^3 \tilde{f}}{\partial y_n^3}\right)\right]_{(0,0)}.
\end{aligned}$$

From the standard N-S bifurcation theory [17,18], we obtain the following theorem.

Theorem 7. *If conditions* (4.10) *hold and* $\hbar \neq 0$, *then system* (1.2) *undergoes a Neimark-Sacker bifurcation at* P_3 *as* δ_* *varies near zero. Moreover, if* $\hbar < 0$ *(respectively,* $\hbar > 0$*), then an attracting (respectively, repelling) invariant closed curve bifurcates from* P_3 *for* $\delta_* > 0$ *(respectively,* $\delta_* < 0$*).*

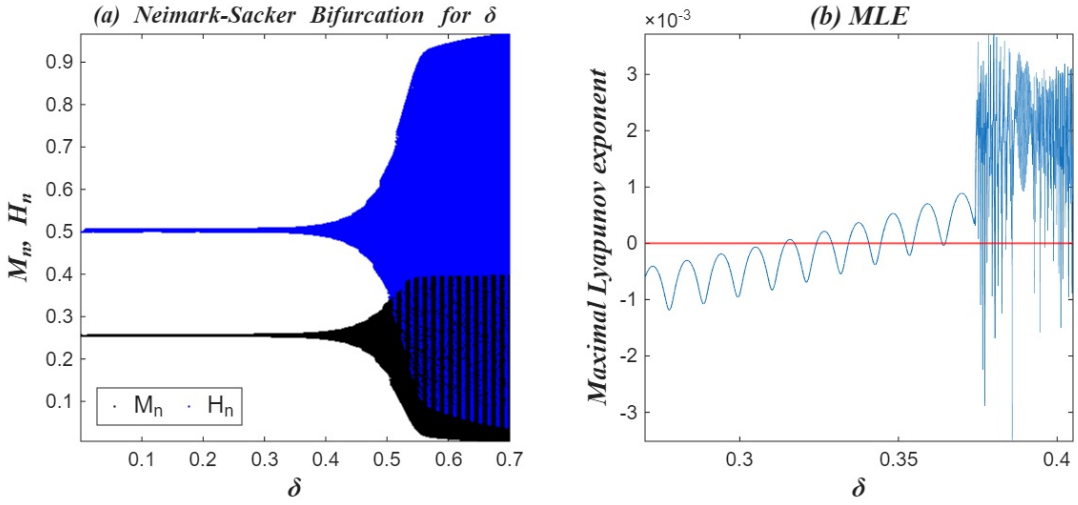

FIGURE 3. Neimark-Sacker diagram and its corresponding Maximal Lyapunov exponent.

Figure (4) provides a comprehensive visualization of how the time step parameter δ affects predator-prey dynamics in a discrete-time model.

Figure (4)(a) Shows temporal evolution of prey population. The Allee effect $\frac{M_n(1-M_n)}{1+\beta M_n}$ creates complex growth patterns, while predation reduces prey density. Larger δ values can lead to overshooting or different equilibrium states.

Figure (4)(b) Shows predator population response. Predator growth is limited by prey availability through the term $M^2+\sigma$, representing the carrying capacity. The coupling with prey dynamics creates characteristic predator-prey oscillations.

Figure (4)(c) Visualizes the system in parameter-state space. Each colored trajectory corresponds to a fixed δ value, showing how the system evolves in the three-dimensional (δ, M_n, H_n) space. The projection of these trajectories reveals relationships between the time step parameter and population densities. we note that the parameter δ acts as a "speed" parameter - larger values lead to faster dynamics but may affect stability, the system shows sensitivity to δ, with different values leading to different equilibrium states, the 3D visualization helps understand how parameter choices δ influence the state space trajectories and the model incorporates biological realism through non-negativity constraints and functional responses.

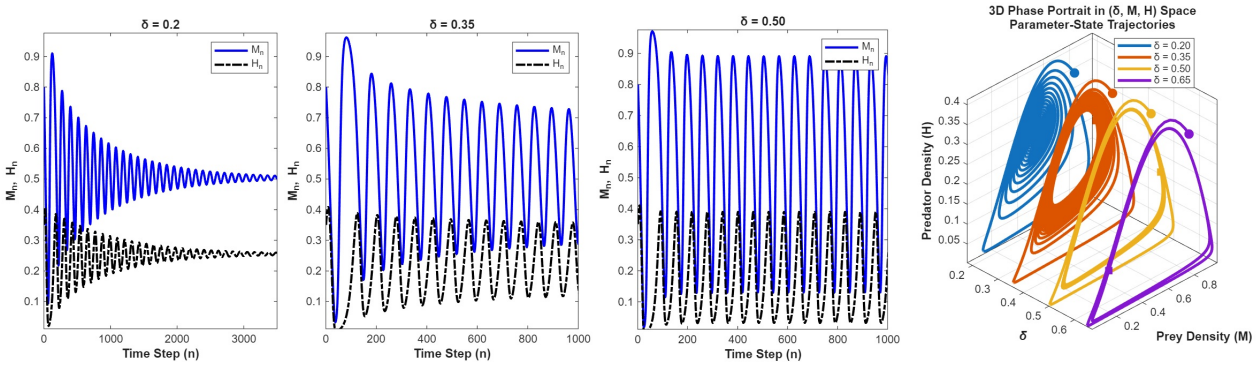

FIGURE 4. Effect of time step parameter δ.

5. Optimal Control Analysis

Optimal control of this predator-prey system provides a mathematical framework for sustainable ecosystem management. By introducing harvesting as a control variable, we apply Pontryagin's maximum principle to derive adaptive strategies that balance economic benefits with ecological stability. The resulting control law activates when immediate harvesting gains exceed the future value of predators, adjusting effort based on real-time population levels. This approach stabilizes oscillatory dynamics, prevents extinction risks, and maximizes sustainable yield. The methodology offers a scientifically-grounded tool for evidence-based conservation and resource management. We introduce a control variable $u_n \in [0, u_{\max}]$ representing predator harvesting effort. The controlled system becomes:

$$\begin{cases} M_{n+1} = M_n + \delta M_n \left(\dfrac{1-M_n}{1+\beta M_n} - \dfrac{\mu H_n}{M_n^2+\sigma} \right), \\ H_{n+1} = H_n + \delta \eta H_n \left(1 - \dfrac{H_n}{M_n^2+\sigma} \right) - u_n H_n, \end{cases} \tag{5.1}$$

with $n = 0, 1, \ldots, N-1$.

To define an objective functional, We consider an economic objective combining harvesting profit with terminal population values:

$$J(u) = \sum_{n=0}^{N-1} \left[Bu_n H_n - \frac{c}{2} u_n^2 \right] + \phi_M M_N - \phi_H H_N, \tag{5.2}$$

where $B > 0$ is unit price for harvested predators, $c > 0$ is cost coefficient for control effort, $\phi_M \geq 0$: terminal value coefficient for prey, $\phi_H \geq 0$ is terminal penalty coefficient for predators.

Define the Hamiltonian at time n:

$$\mathcal{H}_n = Bu_n H_n - \frac{c}{2} u_n^2 + \lambda_{1,n+1} f_1(M_n, H_n) + \lambda_{2,n+1} f_2(M_n, H_n, u_n), \tag{5.3}$$

where:

$$f_1(M_n, H_n) = M_n + \delta M_n \left(\frac{1 - M_n}{1 + \beta M_n} - \frac{\mu H_n}{M_n^2 + \sigma} \right),$$

$$f_2(M_n, H_n, u_n) = H_n + \delta \eta H_n \left(1 - \frac{H_n}{M_n^2 + \sigma} \right) - u_n H_n.$$

And the costate variables $\lambda_{1,n}, \lambda_{2,n}$ satisfy:

$$\lambda_{1,n} = \frac{\partial \mathcal{H}_n}{\partial M_n} = \lambda_{1,n+1} \frac{\partial f_1}{\partial M_n} + \lambda_{2,n+1} \frac{\partial f_2}{\partial M_n}, \tag{5.4}$$

$$\lambda_{2,n} = \frac{\partial \mathcal{H}_n}{\partial H_n} = Bu_n + \lambda_{1,n+1} \frac{\partial f_1}{\partial H_n} + \lambda_{2,n+1} \frac{\partial f_2}{\partial H_n}, \tag{5.5}$$

with terminal conditions:

$$\lambda_{1,N} = \frac{\partial \Phi}{\partial M_N} = \phi_M, \quad \lambda_{2,N} = \frac{\partial \Phi}{\partial H_N} = -\phi_H,$$

where $\Phi(M_N, H_N) = \phi_M M_N - \phi_H H_N$.

The required partial derivatives are:

$$\begin{aligned}
\frac{\partial f_1}{\partial M_n} &= 1 + \delta \left[\frac{1 - M_n}{1 + \beta M_n} - \frac{\mu H_n}{M_n^2 + \sigma} \right] + \delta M_n \left[\frac{-(1 + \beta M_n) - \beta(1 - M_n)}{(1 + \beta M_n)^2} + \frac{2\mu M_n H_n}{(M_n^2 + \sigma)^2} \right], \\
\frac{\partial f_1}{\partial H_n} &= -\delta M_n \frac{\mu}{M_n^2 + \sigma}, \\
\frac{\partial f_2}{\partial M_n} &= \delta \eta H_n \cdot \frac{2 M_n H_n}{(M_n^2 + \sigma)^2}, \\
\frac{\partial f_2}{\partial H_n} &= 1 + \delta \eta \left(1 - \frac{H_n}{M_n^2 + \sigma} \right) - \delta \eta H_n \cdot \frac{1}{M_n^2 + \sigma} - u_n.
\end{aligned} \tag{5.6}$$

The optimal control u_n^* satisfies the stationarity condition:

$$\frac{\partial \mathcal{H}_n}{\partial u_n} = BH_n - cu_n - \lambda_{2,n+1} H_n = 0, \tag{5.7}$$

which yields:

$$u_n^* = \max \left(0, \min \left(u_{\max}, \frac{B - \lambda_{2,n+1}}{c} H_n \right) \right). \tag{5.8}$$

The optimal control problem reduces to solving:

$$\text{State equations (forward):} \quad \begin{cases} M_{n+1} = f_1(M_n, H_n), \\ H_{n+1} = f_2(M_n, H_n, u_n^*), \end{cases} \quad n = 0, \ldots, N-1, \tag{5.9}$$

$$\text{Costate equations (backward):} \quad \begin{cases} \lambda_{1,n} = \lambda_{1,n+1} \frac{\partial f_1}{\partial M_n} + \lambda_{2,n+1} \frac{\partial f_2}{\partial M_n}, \\ \lambda_{2,n} = B u_n^* + \lambda_{1,n+1} \frac{\partial f_1}{\partial H_n} + \lambda_{2,n+1} \frac{\partial f_2}{\partial H_n}, \end{cases} \quad n = N-1, \ldots, 0, \tag{5.10}$$

$$\text{Boundary conditions:} \quad \begin{cases} M_0, H_0 \text{ given}, \\ \lambda_{1,N} = \phi_M, \quad \lambda_{2,N} = -\phi_H. \end{cases} \tag{5.11}$$

6. Numerical Simulation

Table 1. Parameters used in the figures.

Figure	δ	η	(M_0, H_0)
(1), (2)	0.27 : 0.405	7.3	$(0.5, 0.2556)$
(3), (4)	0 : 0.7	0.2	$(0.5, 0.2556)$
(5), (7), (6)	0.63	0.19	$(0.8, 0.35)$

In this section, we will study the behaviors of model (1.2) numerically based on the analysis introduced in the previous sections.

Because most fractional-order differential equations lack exact analytic solutions, approximation and numerical techniques must be used.

The parameters of all figures are $a = q = 1.2$, $\beta = 1$ and initial condition is $(\sigma, \mu, \beta) = (0.002, 0.3, 1.3)$ in this case $P_3 = (0.5036, 0.2556)$ and other parameters in Table (1), Some of the parameters for optimal control have been listed in a Table (2).

Figure (5) below shows the system's behavior in the phase plane (M-H space) comparing uncontrolled dynamics (left) with optimally controlled dynamics (right).

Table 2. Some parameters used in the optimal control figures (5), (7), and (6).

Parameter	**Value**	**Represents**
B	1	Benefit per predator harvested
c	0.5	Cost coefficient
$\boldsymbol{\phi_M}$	0.1	Terminal value for prey
$\boldsymbol{\phi_H}$	0.05	Terminal penalty for predators
$\mathbf{u_{max}}$	0.3	Maximum control

This panel demonstrates the effect of optimal predator harvesting. The control alters the vector field, particularly in predator-dense regions, guiding the system toward a more desirable ecological state. Note how the trajectory differs from the natural oscillation pattern, often reaching a different equilibrium or following a modified path.

Figure (5)(a) shows the natural predator-prey dynamics. The trajectory typically exhibits cyclic oscillations

characteristic of Lotka-Volterra type systems. The vector field reveals equilibrium points where arrows converge (stable equilibria) or diverge (unstable equilibria). Figure (5)(b) System with optimal control, the modified vector field shows how control alters system dynamics, the red trajectory shows the controlled path to desired state.

Figure (5) provides a comprehensive time-domain analysis including population dynamics, control signals, marginal values (costates), and overall performance. This figure helps understand how populations evolve under optimal control, when and how much control to apply, the economic/ecological trade-offs represented by costate variables and the quantitative outcome of the control strategy. Figure (5)(a) compares prey population evolution. Control typically allows prey populations to reach higher or more stable levels by reducing predator pressure. The trade-off between immediate harvesting benefits and long-term ecosystem balance is reflected in the trajectory. In figure (5)(b) predator population response to control. Optimal harvesting reduces predator numbers strategically, not eliminating them completely, but maintaining them at levels that balance ecosystem health and harvesting benefits.

In figure (5)(c) The control signal reveals the optimal harvesting strategy. Typically, control is applied more intensively when predator populations are high relative to prey, and reduced when the system approaches desired equilibrium. Note how control adapts to system state. In figure (5)(d) costate variables represent the marginal value of each population in the objective function. λ_1 (predator value) typically becomes negative, indicating that additional predators have negative value (prompting removal). The difference $B - \lambda_1$ determines control intensity (see Eq. (5.10).

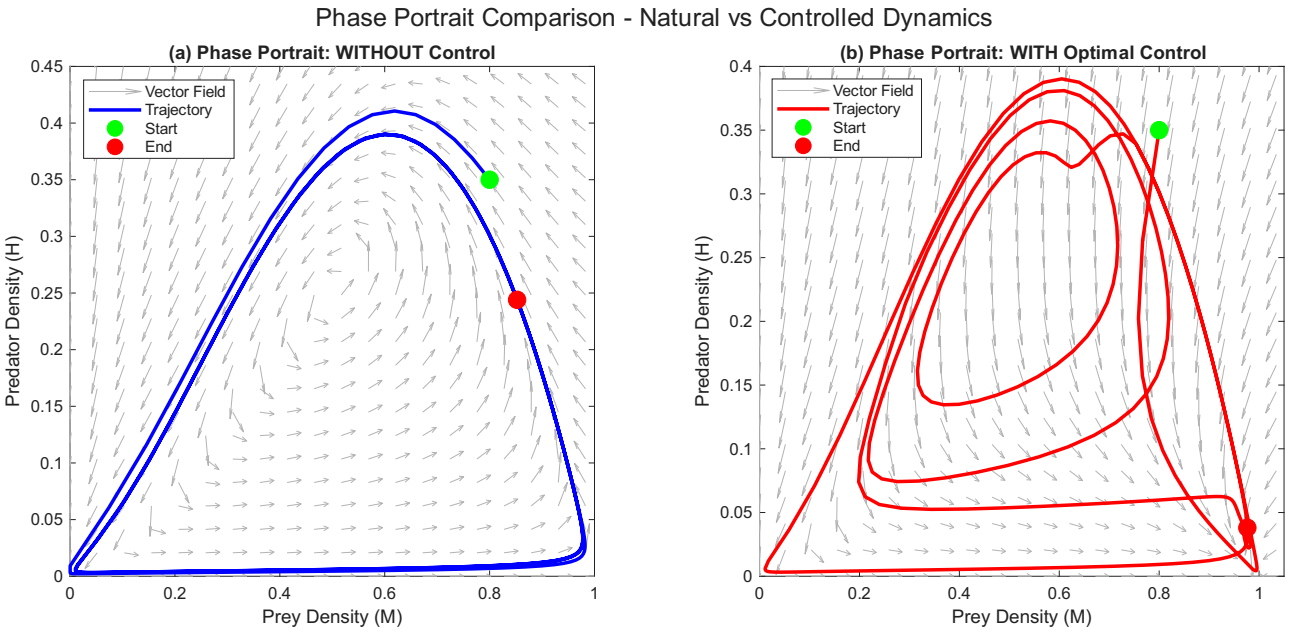

FIGURE 5. Phase portrait comparison.

In figure (5)(e) direct comparison of trajectories shows how control alters the system's path in phase space. The controlled trajectory often takes a different route to potentially reach a different equilibrium or maintain populations within desired bounds.

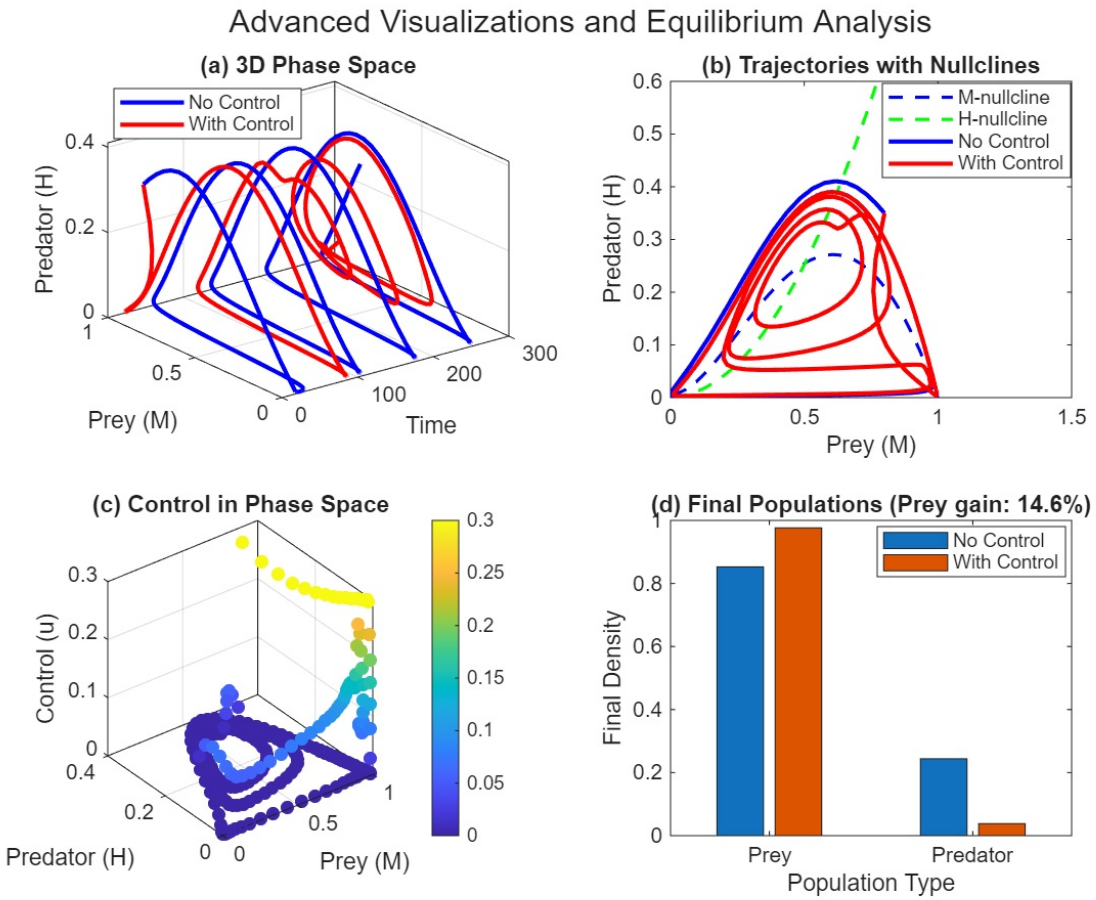

FIGURE 6. Advanced visualization and nullcline analysis.

In figure (5)(f) the objective value quantifies the success of the control strategy. It combines immediate harvesting benefits (BuH), control costs ($\frac{cu^2}{2}$), and terminal values of populations. Higher J indicates better performance according to the specified management objectives.

Figure (6) provides advanced analysis tools: 3D visualization of time evolution, nullcline analysis revealing system equilibria, phase-space representation of control strategy, and quantitative outcome comparison. These visualizations help understand: the temporal-spatial evolution of the system, the underlying equilibrium structure, how control depends on system state and the net effect of control on final population levels. Figure (6)(a) shows how trajectories evolve in the combined time-state space. The spiral patterns indicate oscillatory behavior. Controlled trajectories often have different oscillation amplitudes, frequencies, or equilibrium levels compared to natural dynamics.

Figure (6)(b) Nullclines show where each population's growth rate is zero. Intersections of nullclines indicate equilibrium points. The M-nullcline (blue dashed) shows prey equilibrium for given predator levels, while the H-nullcline (green dashed) shows predator equilibrium for given prey. Controlled trajectories may approach different equilibria or limit cycles. Figure (6)(c) shows control intensity as a function of current

system state. Typically, control is highest when predator density is high relative to prey (upper left region). The color gradient shows how control adapts to different ecological conditions.

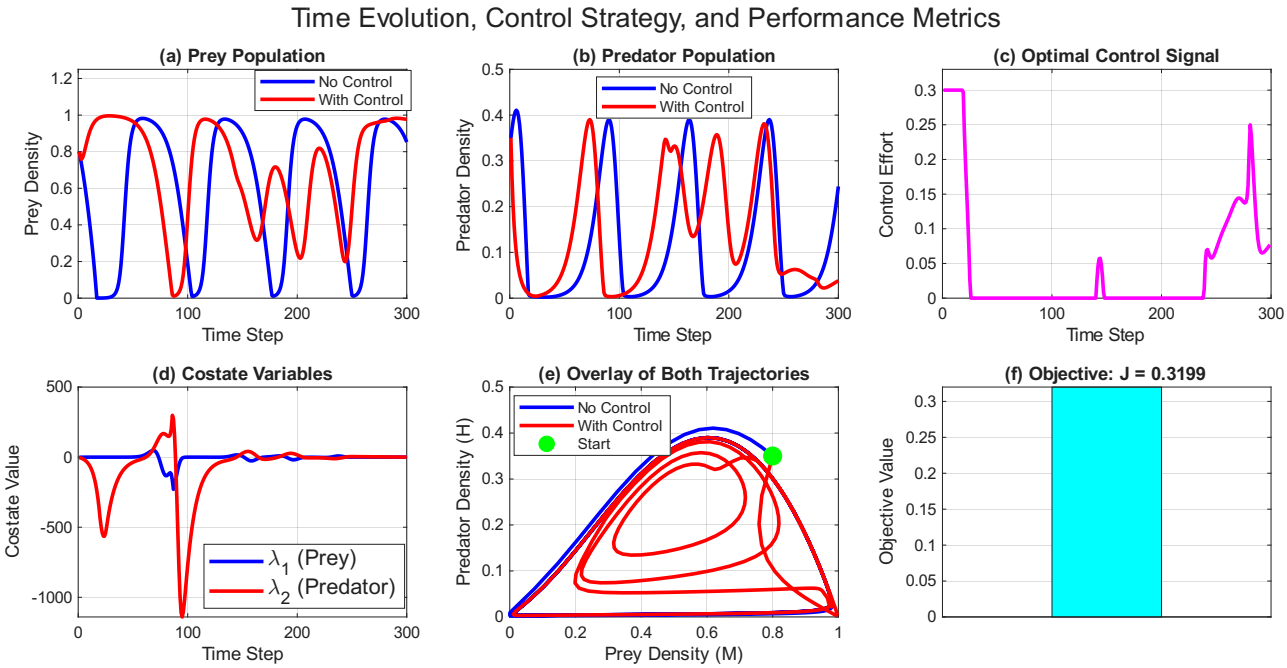

FIGURE 7. Population dynamics over time and the control strategy

Figure (6)(d) bar chart comparing final population levels. Optimal control typically increases prey populations (conservation benefit) while reducing predator populations (harvesting objective). The percentage gain shows the relative improvement in prey population due to control.

7. Conclusions and Future Perspectives

This study has performed an exhaustive examination of a discrete-time predator-prey model characterized by Smith-type growth and Monod-Haldane functional response. We have clarified the intricate dynamic behaviors intrinsic to this ecologically valid system by the utilization of both analytical and numerical approaches. Our stability analysis identified three biologically significant equilibrium states: complete extinction, predator-free equilibrium, and coexistence equilibria. The local stability requirements that come from linearization and the Jury criteria show the ranges of parameters where the system changes from extinction to stable coexistence to oscillatory regimes. The bifurcation analysis showed that changes in ecological parameters lead to different kinds of changes in the system. We found flip bifurcations that show where invasions and extinctions happen, as well as Neimark-Sacker bifurcations that cause oscillations that are almost periodic. Numerical simulations validated these theoretical predictions, demonstrating period-2 orbits, chaotic attractors, and intricate basin geometries. The highest Lyapunov exponent confirmed chaotic regimes, showing how sensitive the system is to its starting conditions.

The optimal control formulation yielded significant management insights. By applying the discrete-time Pontryagin maximum principle, we derived an adaptive harvesting strategy characterized by:

$$u_n^* = \max\left(0, \min\left(u_{\max}, \frac{B - \lambda_{2,n+1}}{c} H_n\right)\right)$$

There are a few important things about this control law: threshold behavior, where harvesting happens when the immediate benefit B is greater than the future value of predators $\lambda_{2,n+1}$; state dependence, where control effort scales with predator density H_n; and an adaptive nature, where the strategy automatically changes to fit changing ecological conditions.

Simulations demonstrated that the best strategy to control oscillatory population dynamics is to make them stable, stop predators from killing prey, keep the yield stable, and make the system more resistant to changes in parameters.The chaotic processes that were observed have significant impacts on ecosystem management. It's tougher to establish long-term projections in chaotic systems, and they might also make it harder to put in place good conservation measures. They can make extinction more likely by making equilibria unstable, which calls for adaptive management methods.Our best way to regulate things indicates, however, that well-planned interventions can help with these issues. The control method provides a fair balance between economic aims (getting the highest production) and environmental restrictions (keeping species alive).

There are a number of useful extensions of this work that need to be looked into more. Fractional-order models add memory effects to make things more realistic from a biological point of view, but also make it harder to analyze and estimate parameters. Stochastic factors account for environmental and demographic unpredictability, whereas spatial dynamics tackle challenges such as habitat fragmentation and dispersal. Pareto-based multi-objective optimization helps find a balance between economic and environmental trade-offs.

Funding: The authors extend their appreciation to Prince Sattam bin Abdulaziz University for funding this research work through the project number (PSAU/2025/01/34227)

Author Contributions: Abdulaziz Almaslokh: Conceptualization, formal analysis, writing-review editing, critical review, funding; B. Alreshidi: Conceptualization, graphic, drawing writing-review editing, critical review; brahim M. E. Abdelstar: Methodology; formal analysis, writing-review editing; A. A. Elsadany: formal analysis, funding, writing-review editing All authors have read and approved the final version of the manuscript for publication.

Conflicts of Interest: The authors declare that there are no conflicts of interest regarding the publication of this paper.

References

[1] A.J. Lotka, Elements of Physical Biology, Williams & Wilkins, Baltimore, 1925.

[2] V. Volterra, Variations and Fluctuations of the Number of Individuals in Animal Species Living Together, ICES J. Mar. Sci. 3 (1928), 3–51. https://doi.org/10.1093/icesjms/3.1.3.

[3] M. Kot, Elements of Mathematical Ecology, Cambridge University Press, 2001. https://doi.org/10.1017/CBO9780511608520.

[4] V.S. Sharma, A. Singh, P. Malik, Bifurcation Patterns in a Discrete Predator–Prey Model Incorporating Ratio-Dependent Functional Response and Prey Harvesting, Qual. Theory Dyn. Syst. 23 (2024), 74. https://doi.org/10.1007/s12346-023-00929-2.

[5] L. Ling, W. Wang, Dynamics of a Ivlev-Type Predator–Prey System with Constant Rate Harvesting, Chaos Solitons Fractals 41 (2009), 2139–2153. https://doi.org/10.1016/j.chaos.2008.08.024.

[6] Z. Eskandari, J. Alidousti, Z. Avazzadeh, J. Tenreiro Machado, Dynamics and Bifurcations of a Discrete-Time Prey-Predator Model with Allee Effect on the Prey Population, Ecol. Complex. 48 (2021), 100962. https://doi.org/10.1016/j.ecocom.2021.100962.

[7] A.P. Maiti, B. Dubey, J. Tushar, A Delayed Prey–Predator Model with Crowley–Martin-type Functional Response Including Prey Refuge, Math. Methods Appl. Sci. 40 (2017), 5792–5809. https://doi.org/10.1002/mma.4429.

[8] S. Gakkhar, A. Singh, B.P. Singh, Effects of Delay and Seasonality on Toxin Producing Phytoplankton–Zooplankton System, Int. J. Biomath. 05 (2012), 1250047. https://doi.org/10.1142/s1793524511001891.

[9] R. Ahmed, A.Q. Khan, M. Amer, A. Faizan, I. Ahmed, Complex Dynamics of a Discretized Predator–Prey System with Prey Refuge Using a Piecewise Constant Argument Method, Int. J. Bifurc. Chaos 34 (2024), 2450120. https://doi.org/10.1142/s0218127424501207.

[10] A. Singh, P. Deolia, Dynamical Analysis and Chaos Control in Discrete-Time Prey-Predator Model, Commun. Nonlinear Sci. Numer. Simul. 90 (2020), 105313. https://doi.org/10.1016/j.cnsns.2020.105313.

[11] A.Q. Khan, A. Maqbool, M.J. Uddin, S.M.S. Rana, Dynamical Analysis of a Two-Dimensional Discrete Predator–Prey Model, J. Comput. Appl. Math. 440 (2024), 115578. https://doi.org/10.1016/j.cam.2023.115578.

[12] M. Mutakabbir Khan, M. Jasim Uddin, D. Fahim, S. Islam, S.M. Sohel Rana, et al., Complex Dynamics of a Discrete Prey–Predator Model with Complex Network and Stochastic Modeling Incorporating a Ratio-Dependent Ivlev Functional Response, Chaos 35 (2025), 033106. https://doi.org/10.1063/5.0248855.

[13] X. Feng, K. Li, M. Liu, L. Wang, T. Wang, Stability and Hopf Bifurcation of a Predator-Prey Model with Smith Growth Rate and Monod–Haldane Functional Response, Adv. Contin. Discret. Model. 2025 (2025), 46. https://doi.org/10.1186/s13662-025-03912-0.

[14] M. Elettreby, Two-Prey One-Predator Model, Chaos Solitons Fractals 39 (2009), 2018–2027. https://doi.org/10.1016/j.chaos.2007.06.058.

[15] Z. Hu, Z. Teng, L. Zhang, Stability and Bifurcation Analysis of a Discrete Predator–Prey Model with Nonmonotonic Functional Response, Nonlinear Anal.: Real World Appl. 12 (2011), 2356–2377. https://doi.org/10.1016/j.nonrwa.2011.02.009.

[16] L.G. Yuan, Q.G. Yang, Bifurcation, Invariant Curve and Hybrid Control in a Discrete-Time Predator–Prey System, Appl. Math. Model. 39 (2015), 2345–2362. https://doi.org/10.1016/j.apm.2014.10.040.

[17] A.A. Elsadany, A.E. Matouk, Dynamical Behaviors of Fractional-Order Lotka–Volterra Predator–Prey Model and Its Discretization, J. Appl. Math. Comput. 49 (2014), 269–283. https://doi.org/10.1007/s12190-014-0838-6.

[18] A.Q. Khan, I. Ahmad, H.S. Alayachi, M.S.M. Noorani, et al., Discrete-Time Predator-Prey Model with Flip Bifurcation and Chaos Control, Math. Biosci. Eng. 17 (2020), 5944–5960. https://doi.org/10.3934/mbe.2020317.